UICHEP-TH-92-14
Fermilab Library
0 1160 0011078 7

UICHEP-TH/92-14

LOGNORMAL MULTIPLICITY DISTRIBUTIONS AND THE DUAL PARTON MODEL

UDAY P. SUKHATME
Department of Physics, University of Illinois at Chicago
Chicago, Illinois 60680, U.S.A.

LIBRARY
SEP 1 1992

ABSTRACT

The multiplicity distributions for proton-proton collisions are computed using the dual parton model and a lognormal function to describe e^+e^- single chain multiplicity distributions. The agreement with pp multiplicity data is very good provided that the valence quark momentum distribution functions in a proton at small-x are taken to be $x^{-\gamma}$, $\gamma \simeq 0.7$, somewhat steeper than the $x^{-1/2}$ behavior used in previous work.

1. Introduction

Several publications in the past two years have shown that lognormal distributions with a generalized form of KNO scaling describe recent e^+e^- multiplicity data very accurately.[1] This is accomplished with just two free parameters over a large energy interval ranging from relatively low values all the way to LEP energies. Previously, it had been shown that multiplicity distributions in hadronic collisions (pp and $\bar{p}p$) could also be well-described by lognormal functions with different parameter values.[2,3] In all cases, the average charged particle multiplicity has a power law behavior $\bar{n} \propto \sqrt{s}^{\alpha}$, characteristic of a branching process. [Other alternative descriptions (negative binomial,[4] Poisson,[5] etc.[6]) also exist, but they usually involve energy-dependent parameters and are less economical].

The dual parton model (DPM) has been successfully used to describe the properties of soft hadronic processes with inputs coming from various types of single chains (q-$\bar{q}$, q-qq, qq-$\bar{q}\bar{q}$).[7] In this paper, we would like to use DPM and the lognormal description of e^+e^- collisions as inputs in order to compute multiplicity distributions for hadronic collisions. Similar approaches have been previously tried[8-11] with other single chain inputs and assumptions. However, at that time, the single chain e^+e^- data was neither as accurately known nor as well parameterized as it is now. The economical and precise description provided by the lognormal distribution will allow us to obtain many simple results about multiplicity moments analytically in addition to reproducing previously expected results.

In Sec. 2, the main features and results of using lognormal distributions for e^+e^- collisions are reviewed. The chief aspects underlying the dual parton model are described in Sec. 3. Finally, in Sec. 4, we insert the single chain inputs of Sec. 2 into DPM in order to compute the multiplicity distributions for proton-proton collisions. The comparison with data is very satisfactory provided that the valence quark momentum

Talk presented at XXII International Symposium on Multiparticle Dynamics, Santiago de Compostela, Spain, July 1992

distribution functions in a proton are taken to be more sharply peaked at $x \simeq 0$ than the usual $x^{-1/2}$ behavior.

2. Lognormal Multiplicity Distributions

2.1 Multiplicity Moments and KNO Plots

Let $P_n(\sqrt{s})$ denote the probability that a collision at center of mass energy $\sqrt{s}$ produces n charged particles. The normalization condition and average multiplicity are given by

$$\sum_n P_n(\sqrt{s}) = 1 \ , \ \bar{n}\,(\sqrt{s}) = \sum_n n P_n\,(\sqrt{s}) \ . \tag{1}$$

The dispersion $D_2\,(\sqrt{s})$ is a measure of the width of the multiplicity distribution. The formula for the generalized dispersion $D_k\,(\sqrt{s})$, $k = 2,3,4, \ldots.$ is

$$D_k(\sqrt{s}) = \left[\overline{(n-\bar{n})^k}\right]^{1/k} \ . \tag{2}$$

Another widely used variety of moments is

$$C_k(\sqrt{s}) = \overline{n^k}/\bar{n}^k \ . \tag{3}$$

Clearly, the higher moments probe the large n tail of $P_n\,(\sqrt{s})$.

Instead of plotting $P_n\,(\sqrt{s})$ vs n, it has become common practice to make KNO plots of $\bar{n}P_n$ vs $z \equiv n/\bar{n}$. This procedure aligns the peaks by re-scaling the horizontal axis and restores the normalization by stretching the vertical axis, giving rise to a much - reduced energy dependence. Exact KNO scaling corresponds to the statement

$$P_n(\sqrt{s}) = \frac{1}{\bar{n}(\sqrt{s})}\ \psi(z) \ , \tag{4}$$

where $\psi(z)$ is an energy-independent function.

2.2 Generalized KNO Scaling and Lognormal Distributions

In the lognormal description,[1,2] it is assumed that the discrete multiplicity distribution $P_n\,(\sqrt{s})$ is obtained from a continuous density function $P(\tilde{n}, \sqrt{s})$ which obeys a generalized KNO scaling.

$$P_n(\sqrt{s}) = \int_n^{n+1} P(\tilde{n},\sqrt{s})\,d\tilde{n} \ , \quad P(\tilde{n},\sqrt{s}) = \frac{1}{\bar{\tilde{n}}(\sqrt{s})}\,\psi(\tilde{z}) \ , \quad \tilde{z} \equiv \frac{\tilde{n}}{\bar{\tilde{n}}} \ , \quad \bar{\tilde{n}}(\sqrt{s}) \equiv \int_0^\infty \tilde{n}\,P(\tilde{n},\sqrt{s})\,d\tilde{n} \ . \tag{5}$$

The function $\psi(\tilde{z})$ is taken to be a lognormal distribution.

$$\psi(\tilde{z}) = \frac{N}{\sqrt{2\pi}\ \sigma\ (\tilde{z}+c)}\ e^{-\frac{[\ln(\tilde{z}+c)-\mu]^2}{2\sigma^2}} \quad . \tag{6}$$

Such a form follows from repeated random branching and occurs in many natural phenomena.[1] The average charged particle multiplicity has the behavior

$$\bar{n}(\sqrt{s}) \sim C\sqrt{s}^{\alpha} \ , \tag{7}$$

and the dispersions D_k are all linearly proportional to $\bar{n}(\sqrt{s})$. Conversely, if such linear dependence is observed for all k, then a lognormal multiplicity distribution is implied.

The data for $\bar{n}$ vs $\sqrt{s}$ is shown in Fig. 1. Eq. (7) gives a good fit to the e^+e^- data for $\sqrt{s} \gtrsim 1$ GeV for $C_{ee} = 2.78$, $\alpha = 0.46$. The pp data is also well-fit by the line shown in Fig. 1 corresponding to $C_{pp} = 1.8$ and the same power $\alpha = 0.46$. Since $C_{pp} < C_{ee}$, this means that pp collisions are much less efficient in particle production than e^+e^- collisions. For example, in order to produce $\bar{n} \simeq 12.8$ charged particles, one typically needs $\sqrt{s} = 64$ GeV pp collisions but only $\sqrt{s} = 32$ GeV e^+e^- collisions. The linear dependence of the dispersions D_2, D_4, D_6 on $\bar{n}$ is shown in Fig. 2 for e^+e^- data. It also holds for pp collisions, but the slopes are greater. The result for D_2 has been known for many years and is called the Wroblewski-Malhotra relation.[12]

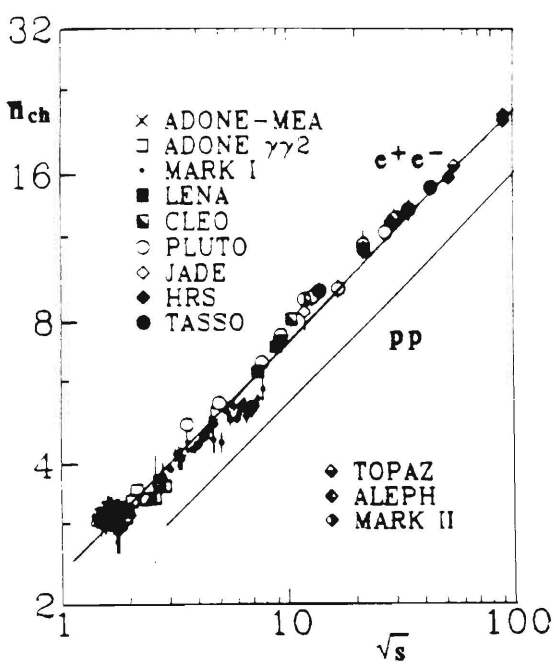

Fig. 1. The average charged particle multiplicity $\bar{n}$ vs CM energy $\sqrt{s}$ for e^+e^- and pp collisions. Only e^+e^- data are shown.

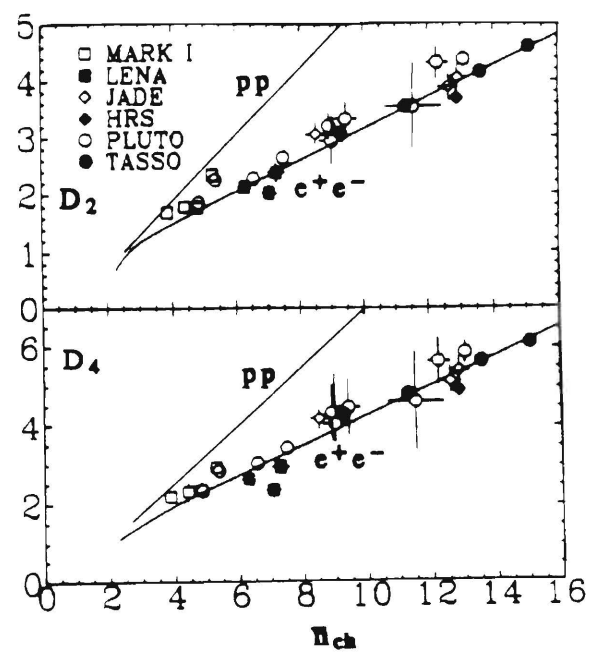

Fig. 2. The dispersions D_2 and D_4 for e^+e^- and pp collisions vs CM energy $\sqrt{s}$. Only e^+e^- data are shown.

3. Dual Parton Model

QCD calculations based on perturbative expansions in the strong coupling constant are not applicable for soft hadronic physics. An alternative promising approach is to use a suitable large-N expansion of QCD, and this naturally gives rise to a topological classification of the contributing graphs. Such a topological expansion, when coupled with the concepts of duality, unitarity, Regge behavior and the parton structure of hadrons, provides the motivation underlying the dual parton model. To date, DPM has had numerous phenomenological successes.[7]

DPM provides a concrete recipe for associating an experimentally observable cross section with each graph in a topological expansion. At high energies, these diagrams involve t-channel exchanges of Pomerons. Multiparticle production is described by making unitarity cuts.

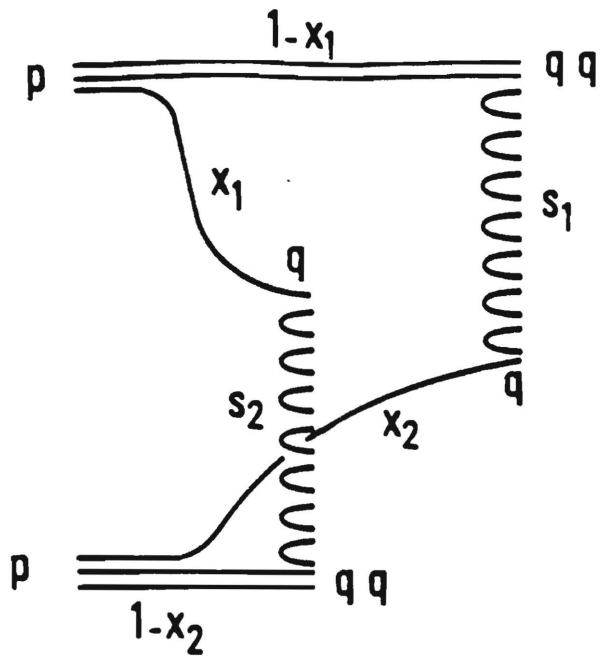

Fig. 3. Single Pomeron exchange (two chain) diagram for pp interactions.

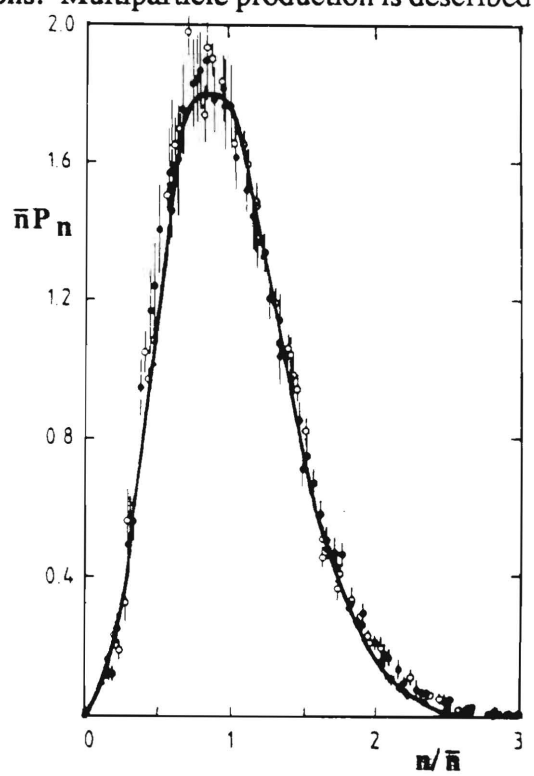

Fig. 4. KNO plot $\bar{n}P_n$ vs $n/\bar{n}$. The curve corresponds to the two chain contribution (Eq. 10). The data is for pp collisions at Fermilab, ISR energies (Ref. 16).

The simplest contribution to the elastic scattering amplitude is a single dual Pomeron, which has the topology of a cylinder. A unitarity cut gives two chains of hadrons (Fig. 3). These chains are stretched between valence quarks of the initial hadrons so as to form color singlets. Similarly, cutting a two Pomeron exchange diagram gives four chains, which end on valence and ocean quarks from the initial hadrons.

To proceed further, we make use of the partonic structure of hadrons, and treat each contributing diagram as a two step process (i) separation of color in the initial collisions, and (ii) fragmentation of colored objects which results in the production of hadronic chains. Consequently, the two ingredients one needs are momentum distribution

and fragmentation functions. For definiteness, let us first consider the leading contribution to multiparticle production in high energy proton-proton (pp) collisions. The collision separates the valence quarks of each incident proton into two colored systems - a quark and a diquark. The fragmentation occurs in the form of two quark-diquark color singlet chains.

In order to make the dual parton model quantitative, it is necessary to specify the probability that the interaction separates the protons into two quarks with momentum fractions x_1 and x_2 and two diquarks with the remaining momentum fractions $(1-x_1)$ and $(1-x_2)$. This probability, which we denote by $\rho(x_1, x_2)$ is taken to be proportional to the valence quark structure functions in a proton.

$$\rho(x_1, x_2) = \nu(x_1)\, \nu(x_2) \ . \tag{8}$$

Structure functions are peaked near $x = 0$, $\nu(x) \sim x^{-\alpha_R(0)}$. This peaked behavior, which follows from Regge considerations, results in two "held-back" quarks near x_1, $x_2 = 0$.

Typically in pp collisions, the "effective" values of x_1 and x_2 are around 0.05.[7] The total energy $\sqrt{s}$ in the overall pp center of mass (CM) frame is shared between the two chains shown in Fig. 3. Let $\sqrt{s_1}$ and $\sqrt{s_2}$ denote the energies of chain 1 and chain 2 in their respective CM frames; we have $s_1 = s\, x_2\, (1 - x_1)$, $s_2 = s\, x_1\, (1 - x_2)$. The rapidity shifts Δ_1 and Δ_2 necessary to go from the overall pp CM frame to the CM of chain 1 and chain 2 are given by $\Delta_1 = (1/2)\ell n[(1-x_1)/x_2]$ and $\Delta_2 = -(1/2)\ell n[(1-x_2)/x_1]$ respectively, and they are essentially independent of energy.

The second ingredient which one needs are quark and diquark fragmentation functions. These can be taken either (i) from hard processes (universality of fragmentation hypothesis) or (ii) from iterative cascade models e.g. Lund model[13] or independent fragmentation model.[14]

The above two ingredients can be readily combined to obtain physically observable quantities. For example, the one Pomeron exchange contribution to the single particle inclusive cross section pp → h + X is given by the superposition of two q-qq chains.

$$\frac{dN}{dy}(s,y) = \int_0^1\!\!\int_0^1 dx_1 dx_2\ \rho(x_1, x_2) \left\{ \frac{dN}{dy}\bigg|_1 (s_1, y-\Delta_1) + \frac{dN}{dy}\bigg|_2 (s_2, y-\Delta_2) \right\} \tag{9}$$

Corrections to the leading single Pomeron (two chain) diagram come from multiple Pomeron exchanges. The weights of these diagrams are fixed by unitarity requirements.[7] Note that the additional chains end on ocean quarks and antiquarks, and hence mainly contribute to multiparticle production in the central region of rapidity. It is clear that each chain must at least have a minimum threshold CM energy in order for physical hadrons to materialize from it. Therefore, on average, up until the highest CERN-ISR energies ($\sqrt{s} < 63$ GeV), the two chain contribution dominates. However, at higher energies (like those at the CERN $\bar{p}p$ collider or the Fermilab Tevatron) there is sufficient energy available to share between four (or more) chains, and multiple Pomeron ex-

changes give an important contribution, and make the central plateau height increase with energy.

4. Multiplicity Distributions for Proton Proton Collisions

4.1 Connecting pp and e^+e^- Moments in DPM

For now, let us focus only on the dominant leading single Pomeron contribution to pp scattering. The multiplicity in any event comes from two q-qq chains, and the multiplicity distribution is given by

$$P_n^{pp}\left(\sqrt{s}\right) = \int dx_1 dx_2\ \rho(x_1, x_2) \sum_{l=0}^{n} P_l^{q-qq}\left(\sqrt{s_1}\right) P_{n-l}^{q-qq}\left(\sqrt{s_2}\right); \sum_n P_n^{pp}\left(\sqrt{s}\right) = 1\ . \quad (10)$$

The average values of n, n^2, ... are given by

$$\bar{n}^{pp}\left(\sqrt{2}\right) = 2 \int dx_1 dx_2\ \rho(x_1, x_2)\ \bar{n}^{q-qq}\left(\sqrt{s_1}\right),$$
$$\overline{n^2}^{pp} = 2 \int dx_1 dx_2\ \rho(x_1, x_2) \left[\overline{n^2}^{q-qq}\left(\sqrt{s_1}\right) + \bar{n}^{q-qq}\left(\sqrt{s_1}\right) \bar{n}^{q-qq}\left(\sqrt{s_2}\right)\right]. \quad (11)$$

Clearly, in order to obtain quantities of interest in pp collisions, one need q-qq chain inputs. We obtain them by making the simplest model relating q-qq and q-$\bar{q}$ chains i.e. we assume that the diquark goes into a baryon (with a flat momentum distribution) and a leftover antiquark. This gives

$$P_n^{q-qq}\left(\sqrt{s}\right) = \int_0^1 dx\ P_{n-\frac{2}{3}}^{q-\bar{q}}\left(\sqrt{sx}\right)\ ,\quad \bar{n}^{q-qq}\left(\sqrt{s}\right) = \frac{2}{3} + \int_0^1 dx\ \bar{n}^{q-\bar{q}}\left(\sqrt{sx}\right). \quad (12)$$

Thus, in a DPM approach, all moments and the multiplicity distributions for pp collisions can be readily expressed in terms of the corresponding quantities for e^+e^- collisions.

4.2 pp Moments from Lognormal Distribution Inputs in e^+e^-

Many of the expressions derived in Sec. 4.1 become much simpler if one uses explicit expressions for $\rho(x_1, x_2)$ from eq. (8) and lognormal distribution inputs from e^+e^- data.

For the valence quark structure functions in a proton, we take the generic form

$$v_p(x) = C_{\gamma p}\ x^{-\gamma}\ (1 - x)^p\ , \quad (13)$$

and use the normalization

$$\int_0^1 v_p(x)\, dx = 1 \quad , \quad C_{\gamma p} = 1/B(-\gamma+1,\, p+1) \; . \tag{14}$$

The standard choice is $\gamma = \alpha_R(0) \simeq ½$ and either p = 3 from dimensional counting rules or p $\simeq$ ⅜ from Regge trajectory considerations.[7]

Substituting for $\bar{n}^{q\text{-}\bar{q}}$ ($\sqrt{s}$) from eq. (7) into eq. (12) yields

$$\bar{n}^{q\text{-}qq}\left(\sqrt{s}\right) = -\frac{1}{3} + C_{qqq}\sqrt{s}^{\alpha} \quad , \quad C_{qqq} = \frac{C_{ee}}{1+\frac{\alpha}{2}} = 2.26 \; . \tag{15}$$

Eq. (11) then gives

$$\bar{n}^{pp}\left(\sqrt{s}\right) = -\frac{2}{3} + 2C_{qqq}(C_{\gamma p})^2 \quad B(-\gamma+\tfrac{\alpha}{2}+1,\, p+1) \quad B(-\gamma+1,\, p+\tfrac{\alpha}{2}+1)\sqrt{s}^{\alpha} \; . \tag{16}$$

Clearly, one is obtaining the same power law behavior $\sqrt{s}^{\alpha}$ for all processes, which as mentioned in Sec. 2.2 is quite consistent with available data. Furthermore, the experimental coefficient $C_{pp} = 1.8$ will agree with the constant appearing in eq. (16) only if the power γ in $v_p(x)$ is properly chosen. One finds $\gamma \simeq 0.70$ for p = 3, $\gamma \simeq 0.76$ for p = ⅜ and an even larger value of γ if p is smaller (as in the Lund Fritiof Monte Carlo).[12] Given the DPM framework, the results for $P_n(\sqrt{s})$ are sensitive to the value of γ, and hence studying multiplicity distributions is a good way to determine γ. For the choice $\gamma = 0.70$ and p = 3, the values of $P_n(\sqrt{s})$ coming from the two chain single Pomeron contribution [eq. (10)] are plotted in Fig. 4. The agreement with experimental data at ISR and lower energies (where higher order multi-chain corrections are unimportant) is remarkably good. One also gets $(D_2/\bar{n})^{pp} \simeq 0.4$.

4.3 Discussion

The universal $\sqrt{s}^{\alpha}$ behavior of average multiplicities and all the dispersions D_k for all processes follows from DPM and the branching character of fragmentation into hadrons. In fact, the two chain diagram of DPM can be regarded as the first step in subsequent e^+e^- type branching. However, the fact that $C_{pp} \neq C_{ee}$ shows that this first step is quite different from subsequent ones. In DPM, the root of this difference is the "held back" effect[7] coming from the peaking of v(x) at small x. Since DPM has at least two chains and $C_{pp} < C_{ee}$, the only way to get this behavior is to make the chain energies $\sqrt{s_1}$, $\sqrt{s_2}$ as small as possible and the rapidities of their centers of mass Δ_1, Δ_2 as large as possible. This is achieved by making γ larger if p is small. Thus, one understands that pp collisions are much less efficient than e^+e^- in producing charged particles since a lot of the incident energy goes into motion of the centers of mass of the two chains.

For describing the rising tail of the multiplicity distribution with energy, one needs to take into account multi-chain diagrams with strengths determined by unitarity.[10] These diagrams contribute more as $\sqrt{s}$ increases, and are known to be responsible for the continuous rise of the central rapidity plateau height with energy and violations of KNO scaling.[15] It is possible that the small bump in the KNO plot at $z \simeq 2$ may be due to the two Pomeron diagram.[15]

5. Acknowledgements

It is a pleasure to thank C. Pajares for a beautifully organized symposium. This work was supported in part by the U.S. Department of Energy.

6. References

1. R. Szwed, G. Wrochna and A. Wroblewski, *Mod. Phys. Lett.* **A5** (1990) 1851 and **A6** (1991) 245.
2. R. Szwed and G. Wrochna, *Z. Phys.* **C29** (1985) 255.
3. M. Gazdzicki, R. Szwed, G. Wrochna and A. Wroblewski, *Mod. Phys. Lett.* **A6** (1991) 981.
4. A. Giovannini and L. Van Hove, *Z. Phys.* **C30** (1986) 391.
5. A. Capella and A.V. Ramallo, *Phys. Rev.* **D37** (1988) 1763.
6. V. Gupta and N. Sarma, *Z. Phys.* **C52** (1991) 53; N. Sarma, contribution to these Proceedings.
7. A. Capella, U. Sukhatme, C-I Tan and J. Tran Thanh Van, *Phys. Lett.* **B81** (1979) 68 and *Z. Phys.* **C3** (1980) 329; H. Minakata, *Phys. Rev.* **D20** (1979) 1656; G. Cohen-Tannoudji et al., *Phys. Rev.* **D19** (1979) 3397 and **D21** (1980) 2689; A. Kaidalov, *Phys. Lett.* **B116** (1982) 459. For a recent review, see A. Capella, U. Sukhatme, C-I Tan and J. Tran Thanh Van, Orsay preprint (1992), submitted to *Physics Reports*.
8. A. Kaidalov and K. Ter-Martirosyan, *Phys. Lett.* **B117** (1982) 247.
9. T. Kanki, *Nucl. Phys.* **B243** (1984) 44.
10. A. Capella and J. Tran Thanh Van, *Z. Phys.* **C23** (1984) 165; A. Capella, A. Staar and J. Tran Thanh Van, *Phys. Rev.* **D32** (1985) 2933.
11. P. Aurenche, F. Bopp and J. Ranft, *Z. Phys.* **C23** (1984) 67 and **C26** (1984) 279.
12. A. Wroblewski, *Acta Phys. Pol.* **B4** (1974) 857; P. Malhotra, *Nucl. Phys.* **B46** (1973) 559.
13. B. Andersson, G. Gustafson, G. Ingelman and T. Sjöstrand, *Phys. Rep.* **97** (1983) 31.
14. A. Krzywicki and B. Petersson, *Phys. Rev.* **D6** (1972) 924; J. Finkelstein and R. Peccei, *Phys. Rev.* **D6** (1972) 2606; R. Feynman and R. Field, *Nucl. Phys.* **B136** (1978) 1; U. Sukhatme, *Phys. Lett.* **B73** (1978) 478.
15. U. Sukhatme, in *Proc. XVI Int. Symposium on Multiparticle Dynamics*, Kiryat-Anavim, Israel (1985), ed. J. Grunhaus.
16. A. Breakstone et al., *Phys. Rev.* **D30** (1984) 528.